CrossMark

ORIGINAL PAPER

Facile Synthesis of Quasi Spherical ZnO Nanoparticles with Excellent Photocatalytic Activity

Manoj Pudukudy · Zahira Yaakob

Abstract   In this article, we report on the synthesis, characterization and photo-catalytic activity of quasi spherical ZnO nanoparticles obtained by an egg white assisted facile sol–gel type wet method. The material was characterized for its structural, textural and optical properties. The hexagonal wurtzite crystalline structure of ZnO with high phase purity was confirmed by the X-ray diffraction analysis. The mesoporous texture generated from the inter-agglomeration of ZnO nanoparticles was clearly shown in the transmission electron microscopy (TEM) images. The N_2 sorption analysis indicated a specific surface area of 18 m^2/g, with monomodal mesoporosity. The optical studies had shown the decreased optical band gap (3.28 eV) of the sample with the existence of a number of crystal defects, especially oxygen vacancies in the sample. The aquatic dye pollutants were effectively degraded under UV irradiation over the ZnO nano photocatalysts. They were also found to be reusable up to five consecutive runs without loss in catalytic activity, indicating their high photostability against photocorrosion.

Keywords   ZnO nanoparticles · Optical properties · Mesoporosity · Photodegradation · Reusability

M. Pudukudy (✉) · Z. Yaakob
Department of Chemical and Process Engineering, Faculty of Engineering and Built Environment, Universiti Kebangsaan Malaysia, 43600 Bangi, Selangor, Malaysia
e-mail: manojpudukudy@gmail.com

M. Pudukudy
Fuel Cell Institute, Universiti Kebangsaan Malaysia, 43600 Bangi, Selangor, Malaysia

Introduction

Aquatic pollution is one of the most serious problems in the world, since it has an adverse effect on the human health and living organisms. The discharge of various hazardous organic compounds especially chemicals, dyes, pesticides, herbicides from various industries to water bodies destroyed the aquatic system. Organic compounds are not bio-degradable; therefore it is highly demanding to find an effective route to degrade the organic compounds [1]. Dyes are one of the most hazardous organic pollutants found in water bodies from the textile industries, and which are accumulating day by day, by their dumping process. Photocatalytic degradation has received much special attention, because it is the easiest, greener and innovative method for the complete degradation organic dyes. The semiconductor nano photocatalysts were found to have a significant role in the treatment of these aquatic pollutants. In recent years, they have received much special attention for the removal of pollutants, due to their enhanced properties differs from those of the bulk materials. Based on this fact, vast studies have been on-going in their synthesis and characterization. Among the various nano semiconductors, ZnO has received a special attention in the area of materials research, since it has wide band gap energy of 3.37 eV and large exciton energy of 60 meV [2]. It has found promising applications in solar cells, ceramic materials, gas sensors, catalysts, UV absorbers, electronic batteries, self-cleaning devices, etc. [3–6]. Numerous synthetic routes have been applied to synthesize the ZnO nanoparticles, including hydrothermal, precipitation, sol–gel, spray pyrolysis, chemical vapor deposition, microwave route, mechanical milling, thermal evaporation, microemulsion, ultra sonication, solid state mixing and so on [7–12]. The nano and micro- structured ZnO with various attracted morphologies such as rods, wires, tubes, belts, flakes, sheets, walls, flowers, cones, tetra pods, granular and plate like structures were fabricated by the aforementioned synthetic methods [13–18]. In addition, the use of surfactants and templates has been explored in this respect, and they were found to contribute a leading role in the improvement of its morphology and properties [19, 20].

Organic templates like di or tri- block copolymers, ionic liquids, and surfactants like urea, citric acid etc. were found to have an enhanced effect on the properties of ZnO [21]. This is mainly due to their effect on the particle size, structure, texture and hence its influence on the physical, chemical, optical and electrical properties [22]. Some of the widely used organic templates are cetyltrimethylammonium bromide (CTAB), polyethylene glycol, triethyl amine, ethylene glycol and diisopropyl amine [23, 24]. However, the role of naturally occurring templates such as proteins, carbohydrates, sugars, etc. was also explored in materials research, but they seem to be less utilized for the synthesis of ZnO. Among the different natural templates, proteins have received an increased attention, since they have the capacity to manage the nucleation, crystallization and properties of inorganic materials [25, 26]. Egg white one of the naturally occurring, ecofriendly green templates with a large amount of proteins. Due to the gelling, foaming and emulsifying characteristics of egg white proteins, its role in the synthesis of nanomaterials is highly significant. Also one of the advantage is that, it can be burnt very easily after the material synthesis [26–28].

In this work, we report on the synthesis, characterization and photocatalytic activity of quasi spherical ZnO nanoparticles obtained by an egg white assisted facile wet method. Even though, the egg white assisted synthesis of ZnO has been already reported by some other researchers [29–31], we obtained highly resolved more or less spherical nanoparticles for the first time, instead of the conventional rod and brush like micro morphologies. The as-prepared ZnO nanoparticles were successfully utilized for the photocatalytic degradation of some aquatic dye pollutants (10 mg/L) under UV irradiation over a low catalyst dose, using air as the potential oxidizing agent.

Experimental

Synthesis of ZnO Nanoparticles

All of the chemicals were of analytical grade and used without further purification. The egg white was taken freshly before starting the experiment. In the typical procedure, 18.5 g of $Zn(NO_3)_2 \cdot 6H_2O$ was first dissolved in 50 mL of distilled water. Then the precursor solution was slowly added into 50 mL of egg white in a large beaker with vigorous stirring until it becomes a white syrupy/foamy paste. After that, it was kept in an oven at 100 °C until it gets dried. Finally the sample was crushed, powdered and calcined at 600 °C for 5 h to obtain the ZnO nanoparticles.

Characterization of ZnO Nanoparticles

The as-synthesized ZnO nanoparticles were characterized by means of various analytical techniques including powder X-ray diffraction (XRD), Fourier transform infrared spectroscopy (FTIR), Field emission scanning electron microscopy (FE-SEM), Energy dispersive spectroscopy (EDS), Transmission electron microscopy (TEM), and Brunauer–Emmett–Teller and Barrett–Joyner–Halenda (BET/BJH) analysis. The XRD analysis was carried out on a Bruker D8 Focus powder diffractometer with Cu Kα radiation wavelength of 0.15406 nm. The samples were scanned from 10° to 80° with a step size of 0.025°. The mean crystalline size of the sample was calculated from the full width at half maximum (FWHM) of the intense X-ray diffraction peaks using Scherrer's equation. The FT-IR spectrum was recorded in transmission mode with a thermoscientific NICOLET 6700 apparatus in the region of 400–4,000 cm^{-1}. The FESEM images for the determination of surface morphology were performed on a Zeiss SUPRA 55 scanning electron microscope. The scanning electron micrographs were obtained at an operating voltage of 3 kV. TEM images for the determination of the internal morphology were performed on a Philips CM-12 instrument at an operating voltage of 100 kV. The porosity and surface area of the sample was determined by nitrogen adsorption–desorption analysis at 77 K using a Micromeritics ASAP 2010 instrument. The specific surface area of the sample was assessed by BET method and the pore size and pore volume distribution was determined by BJH method. The optical properties of the sample were studied using UV–Visible and photoluminescence spectroscopy. The photoluminescence spectrum

of the sample was taken in a FLSP920 Edinburgh Instrument with 450 W Xenon lamp as the radiation source and an excitation wavelength of 300 nm. The UV–Visible absorbance spectrum was recorded in a Perkin–Elmer Lambda-35 (Varian Cary) spectrophotometer using water as the reference solvent.

Photocatalytic Measurements

The photocatalytic activity of the as-prepared ZnO nanoparticles was evaluated by the degradation of a model dye pollutant, methylene blue (MB). The photocatalytic experiments were carried out in a photoreactor (Rayonet type Photoreactor, Associate Technica, India) with 16, 8 W, UV lamps (Hitachi 8Watt, Hittach, Ltd., Tokyo, Japan, irradiation wavelength (λ) of 352 nm). In each experiment, 0.05 g of ZnO photocatalyst was dispersed in 50 mL of methylene blue solution with a concentration of 10 mg/L. Before irradiation, the solution was kept in the dark for 20 min with proper aeration, in order to establish adsorption–desorption equilibrium prior to the photodegradation [32]. After that, the suspension was irradiated under UV light with continuous air bubbling as the potential oxidizing agent for different irradiation time. After the completion of the each reaction, the solution was quickly centrifuged and its absorbance spectrum was recorded to calculate the percentage of degradation. The photodegradation efficiency was calculated according to the following equation: Degradation (%) = $((A_0 - A)/A_0) \times 100$ %, where A_0 represents the initial absorbance of the dye solution and A represents the absorbance after UV irradiation.

Results and Discussion

Material Characterization

The crystalline structure and phase purity of the as-synthesized samples were investigated by XRD and the results are shown in Fig. 1. No clear diffraction peaks were observed in the noisy spectrum of the dried sample (Fig. 1a), indicating its amorphous character due to the presence of organic egg white residues [29]. However, some weak and less intense peaks were observed at the 2θ values from 30° to 40°, which can be due to the presence of minor crystalline phase of Zn-egg white organo-inorganic complexes. The XRD pattern of the sample calcined at 600 °C is shown in Fig. 1b, where the miller indices of peaks are marked. It can be seen that, all of the diffraction peaks at the 2θ values of 31.3°, 34.8°, 36.4°, 48.2°, 57.0°, 63.2° and 68.3° were directly indexed to the phase pure hexagonal wurtzite crystalline structure of ZnO with the lattice parameters of a = 3.250 Å and c = 5.206 Å and P6$_3$mc space group (JCPDS Card No.: 36-1451). The sharp and clear diffraction peaks indicate that the ZnO has high crystalline quality. No other typical peaks of impure phases were observed. The full width at half maximum (FWHM) of the diffraction peak at 36.4° was used to calculate the crystalline size and the value was found to be approximately 30 nm.
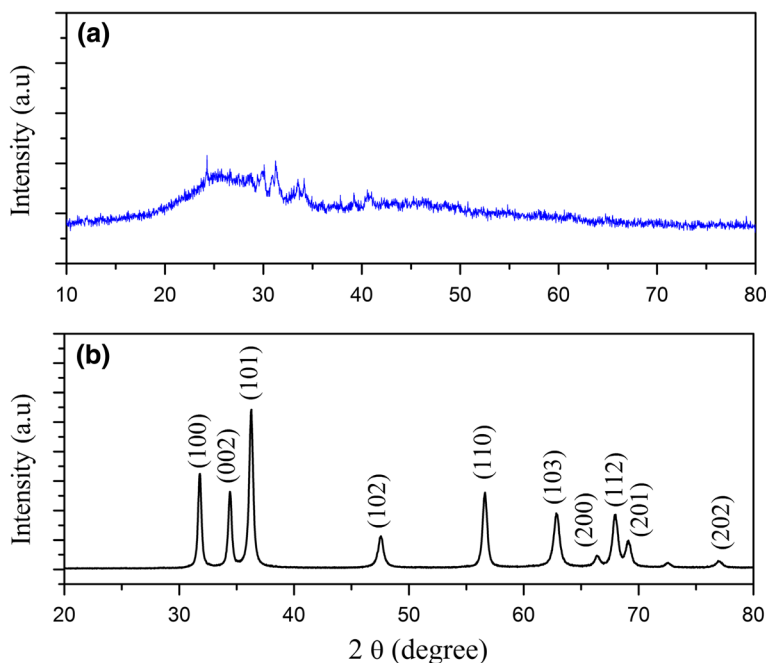
Fig. 1 XRD patterns of the **a** dried sample and **b** calcined at 600 °C

The surface composition of the calcined sample was studied by FTIR and the spectrum is shown in Fig. 2a. The well resolved intense and broad transmission band centered at ∼488 cm^{-1} was attributed to the stretching vibration of zinc-oxygen bond [33]. This further confirms the formation of ZnO. No other bands related to the egg white residue were observed in the spectrum, indicating the complete removal of egg white by annealing at 600 °C. The elemental composition of the calcined sample was studied by EDS analysis and the spectrum is shown in Fig. 2b. It only showed the presence of Zn and O as elements, without any other elemental contamination. The atomic weight ratio of Zn and O shown in the inset table indicates that, there is sufficient amount of oxygen vacancies in the sample [34].

The morphology of the as-synthesized ZnO was examined by FESEM and the images at different magnifications are shown in Fig. 3. It can be seen that all the particles were in more or less spherical shape with a wide particle size distribution of 30–90 nm with well separated grain boundaries. The particles were found to be homogenously aggregated, resulting in the formation of a hierarchical sheet like appearance. The internal structure of the ZnO nanoparticles was investigated by TEM and images are shown in Fig. 4. Here we saw the homogeneously aggregated spherical ZnO nanoparticles with the typical size of 30-35 nm and the observed size is found to be in good agreement with the XRD result. Many of the ZnO nanoparticles were appeared to be quasi-spherical. The empty or inter spaces
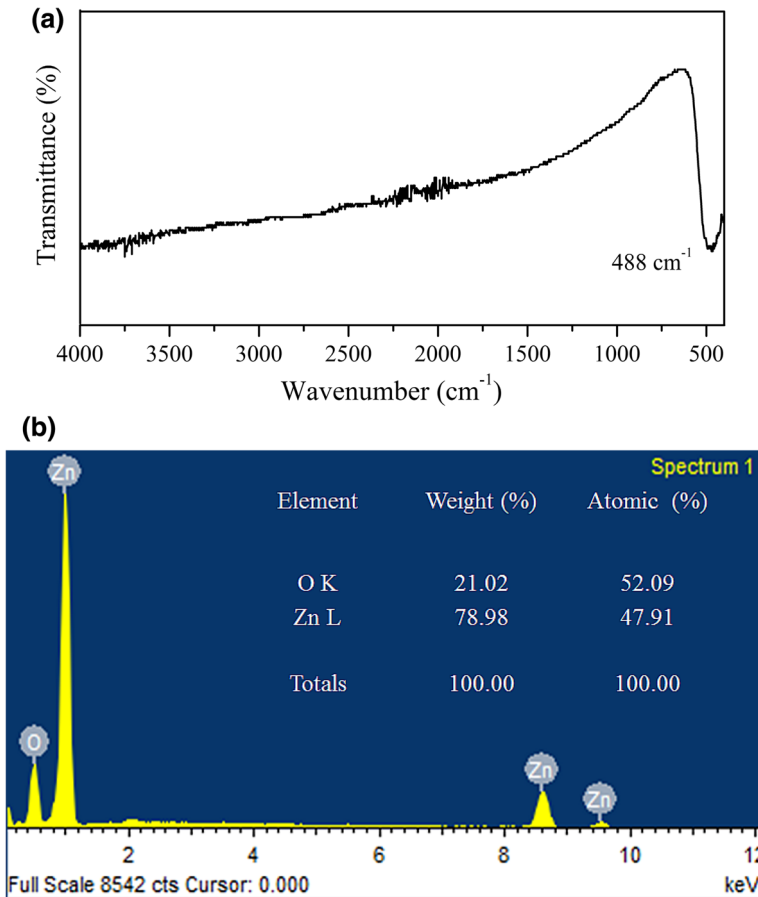
Fig. 2 **a** FTIR spectrum of the ZnO and **b** its EDS spectrum

between the particles were marked in Fig. 4c, d and these are considered to be the pores generated by the inter-agglomeration of ZnO nanoparticles.

BET/BJH analyses were done to study the textural properties of the ZnO nanoparticles. The nitrogen adsorption–desorption isotherm of the sample is shown in Fig. 5. It is a type IV isotherm with H3 hysteresis loop (observed in the P/P_0 range of 0.8–0.95), indicates that the sample has a mesoporous texture with slits-like pores [35, 36]. The specific surface area calculated by the BET method was found to be 18 m^2/g and BJH plot was used to evaluate the pore size distribution of the sample. The inset figure in Fig. 5 represents the BJH desorption cumulative pore size curve and which confirms the presence of uniform pores (~ 25 nm) and a monomodal mesoporosity in the sample [37].

The role of egg white in the synthesis of ZnO nanoparticles can be explained as follows. The proteins present in the egg white interact with the Zn^{2+} ions in solution and some organo-inorganic zinc complexes were formed in the course of stirring,
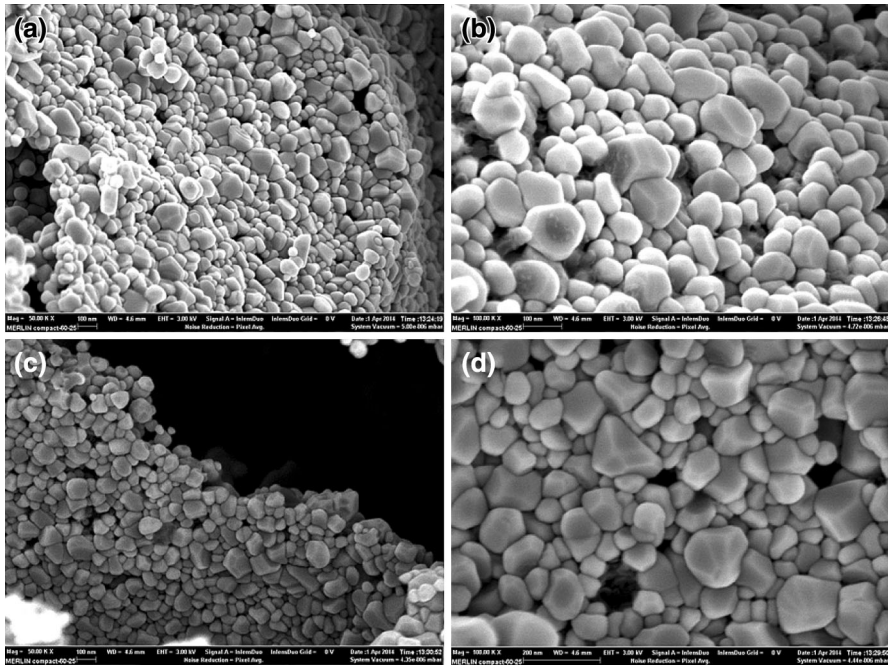
Fig. 3 FESEM images of the ZnO nanoparticles

since they have a very high affinity for metal ions [26]. Due to the physical stress aroused by the stirring, the proteins present in the egg white get denatured and coagulated to syrupy foam by the presence of hydrophobic and hydrophilic amino acids present in it. This is mainly due to the change in the ionic strength and increased pH of the solution as reported previously [38]. Based on the preferential adsorption of these organic groups on the plane of crystals, their growth on that particular plane can be retarded during the thermal treatment [39] and which results in the formation of more or less spherical ZnO nanoparticles. The particle size variation observed in the FESEM images can be attributed to the non-uniformity of the adsorption of organic groups on the surface of ZnO crystallites. Here, the proteins serve as directors during the nucleation, growth, and assembly of ZnO nanocrystallites and act as a nanoreactor for the growth of ZnO nanopartiles [40]. The release of huge amount of gas from the bulk of the dried sample by the rapid burning of egg white, introduces tight spaces in between the particles and which provides a porous network to the ZnO sample [41].

The optical properties of the ZnO nanoparticles were studied using UV–Visible and photoluminescence (PL) spectroscopy. The UV–visible absorbance spectrum of the ZnO nanoparticles dispersed in water is shown in Fig. 6. The absorption peak centered at $\sim$378 nm is the characteristic peak for hexagonal wurtzite ZnO [42]. The absorption peak shows a red shift of about 19 nm compared to that of bulk ZnO (365 nm) [43]. This red shift can be attributed to the development of shallow levels
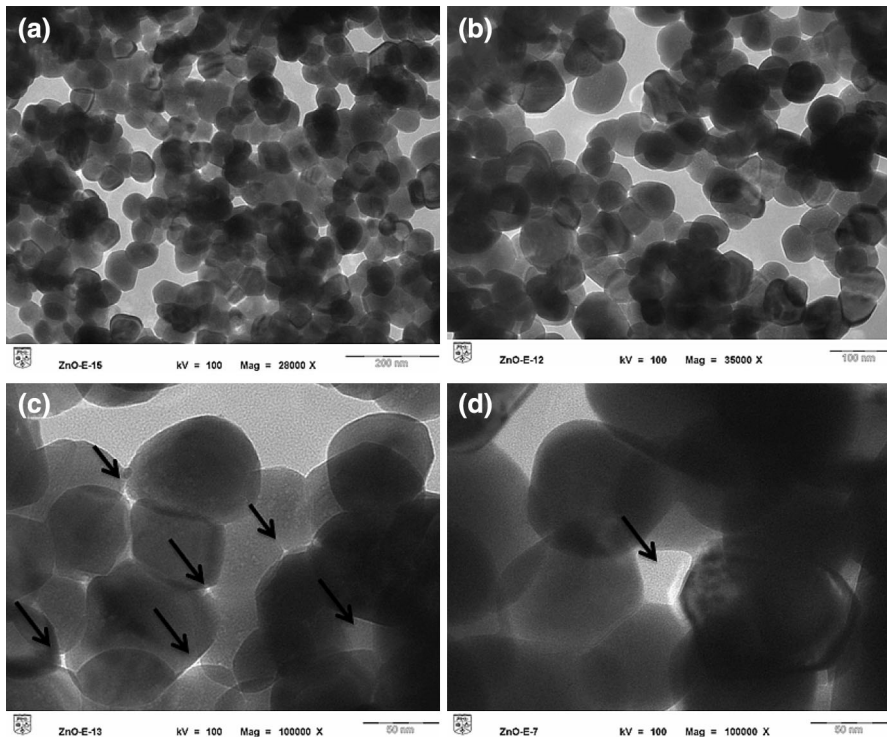
Fig. 4 TEM images of the ZnO nanoparticles at different magnifications

inside the band gap due to the presence of foreign atoms in the lattice [44]. The shift of the absorption peak to higher wavelength indicates the decrease of optical band gap (1st bright exciton energy) [45, 46]. The optical band gap was calculated based on the equation E_g (eV) $= (hc/\lambda) = 1,240/\lambda$ (nm), where E_g is the optical band gap, h is the Planck's constant, c is the speed of light and λ is the wavelength of maximum absorption. The calculated optical band gap value is found to be 3.28 eV and lower than that of the bulk ZnO (3.37 eV). The decreased optical bang gap can be due to the quantum confinement effects and the presence of intrinsic crystal defects [44].

To investigate the crystal defects, the photoluminescence spectrum was taken and the result is shown in Fig. 7. The emission bands were found to be observing in the blue-green region. The absence of emission band at $\sim$397 nm indicates the absence of exciton related near-band edge emission, generated by the recombination of electrons and holes formed the by light irradiation [47]. The deep level emissions were clearly observed in the sample and which were located in the blue-green region. The blue bands centered at around 412, 439, 451, 468, 482 and 493 nm, and green yellow emission bands observed at 554 and 617 nm were attributed to the presence of intrinsic crystal defects in the ZnO nanoparticles [48]. The intrinsic defects mainly comprise oxygen and zinc vacancies present in the lattice and
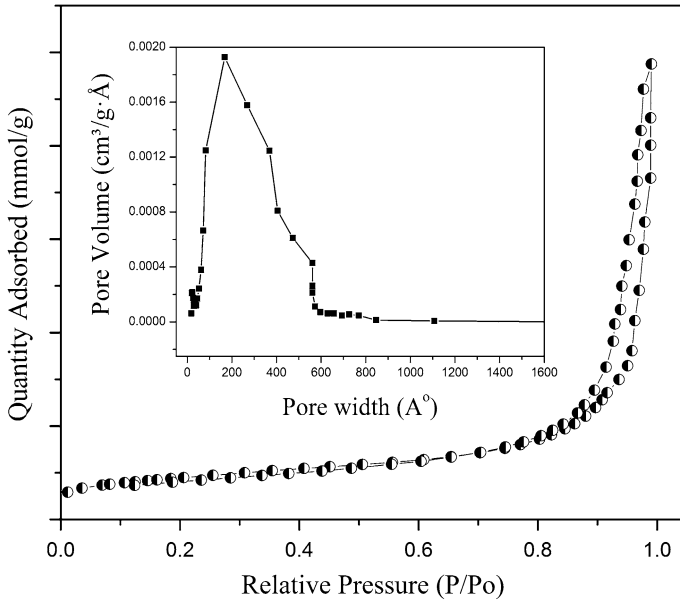
Fig. 5 Nitrogen sorption (BET) isotherms of the ZnO nanoparticles and BJH plot (*inset* figure)
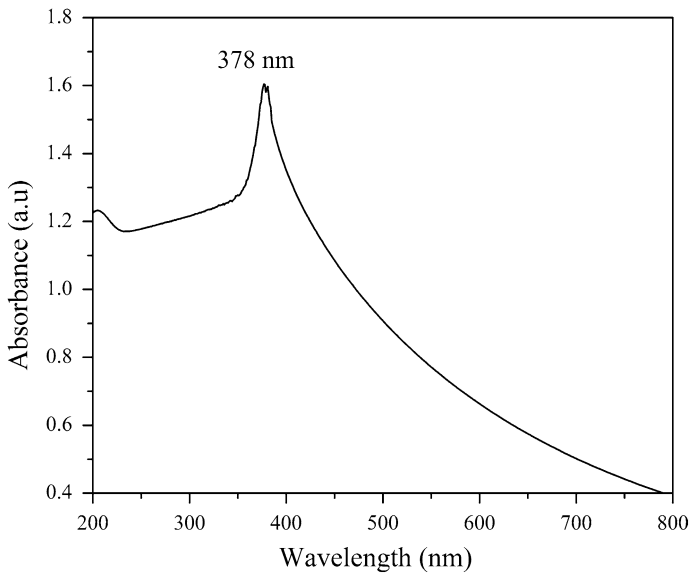

Fig. 6 UV–Visible optical absorption spectrum of the ZnO nanoparticles

interstitial sites of the crystal [49, 50]. The broad and intense green-yellow emission bands centered at 554 nm and 617 nm was arisen due to the presence of singularly ionized oxygen vacancies [51]. These oxygen vacancies were attributed to the

radiative recombination of a photo generated hole with an electron occupying the oxygen vacancy, as reported by Kiomarsipourn and Razavi [52]. The high intensity of these visible emission bands interprets that the sample has high oxygen vacancies and which lowers the rate of electron hole pair recombination in the sample. The inset table in the EDS spectrum shown in Fig. 2b, supports this observation [53].

Photocatalytic Activity

To validate the potential environmental application of the as-synthesized ZnO nanoparticles, their photocatalytic activity was investigated. The photocatalytic degradation of hazardous dye pollutant methylene blue was selected to monitor the catalytic activity of the quasi-spherical ZnO nanoparticles. Without any photocatalyst, a slow decrease in the concentration of methylene blue was observed under UV light irradiation as shown in Fig. 8. Only 8–9 % noncatalytic self-degradation of methylene blue was observed under UV light irradiation with continuous air bubbling for 60 min. However, the addition of ZnO nanoparticles increased the degradation rate drastically. Within 10 min, 72 % of dye removal was noticed, which is found to be very high compared to several recent reports. However, the complete degradation of MB (50 mL 10 mg/L) was observed after 55 min. The changes in the optical absorbance spectra of the MB solution with different irradiation time intervals are shown in Fig. 9a. It can be seen that the maximum absorbance of MB at 663 nm diminishes rapidly with increasing the irradiation time and the absorbance peak become completely removed after 50 min, which is due to the complete destruction of homocyclic and heterocyclic aromatic rings present in the dye molecules by photodegradation [54]. To study the kinetics of methylene blue photodegradation, the first order rate equation was used [32, 55]. The rate equation is given by the expression: $\ln (C_o/C) = K\,t$, where K is the rate constant in time^{-1}, C_o is the initial concentration of the MB and C is the concentration after the irradiation time 't' in minutes. Using the slope of a linear plot of $\ln (C_o/C)$ versus t shown in Fig. 9b, the rate constant (K) was calculated to be 0.158 min^{-1}.

The photocatalytic degradation mechanism over the ZnO nano photocatalysts can be explained as follows. The irradiation of UV-light with proper or higher than the band gap energy of ZnO creates an electron–hole pair by the transfer of electrons from valence band (VB) to the conduction band (CB). These as-generated holes and photoelectrons migrate to the surface of ZnO and reacts with water and oxygen in the solution to create reactive radical species such as hydroxyl and superoxide anion radicals, responsible for the degradation of dyes [56]. The hydroxyl radicals are formed by the oxidation of water with holes in the valence band, whereas the superoxide anion radicals are generated by the reduction of oxygen with electrons present in the conduction band. The superoxide anion radicals again react with water and produce more OH radials. These radicals actively participate in the degradation of dye molecules [57].

Photostability of the ZnO nanoparticles for dye degradation was investigated by the reusability experiments. The used ZnO photocatalysts were collected, washed with distilled water, dried and utilized further for the photodegradation of MB and the results are shown in Fig. 10. The ZnO nanoparticles were found to be effectively
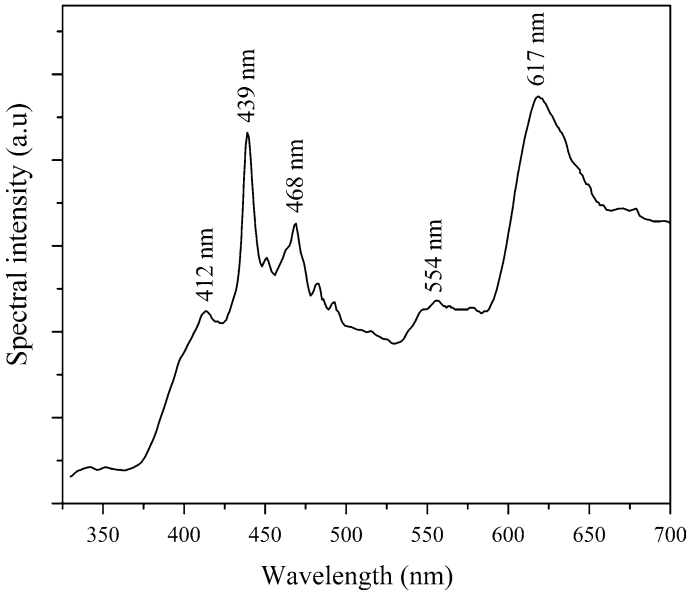
Fig. 7 Room temperature photoluminescence spectrum (PL) of the ZnO nanoparticles
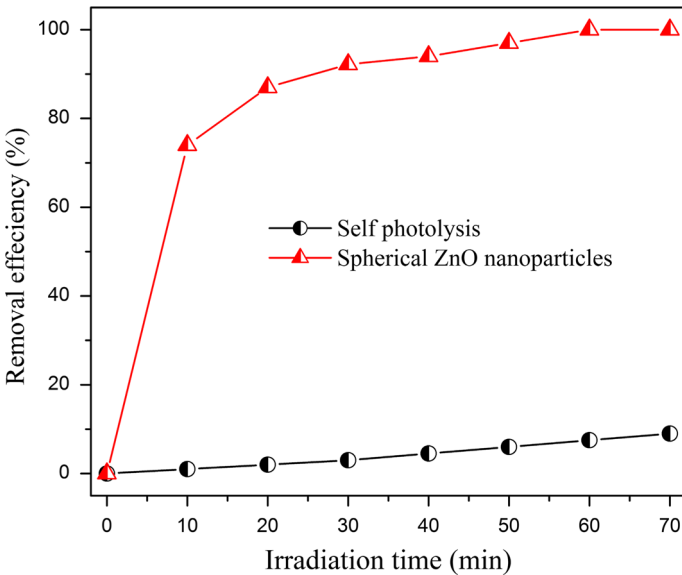

Fig. 8 Photodegradation efficiency of the ZnO nanoparticles (50 mL 10 mg/L MB solution, 0.05 g ZnO and constant air bubbling under UV light irradiation)

reusable for five successive runs. Up to third run, no diminishing effect was noted for dye degradation. But after the fourth run, the activity was dropped to 85 %, which is attributed to the loss of photocatalyst during the catalyst recovery steps
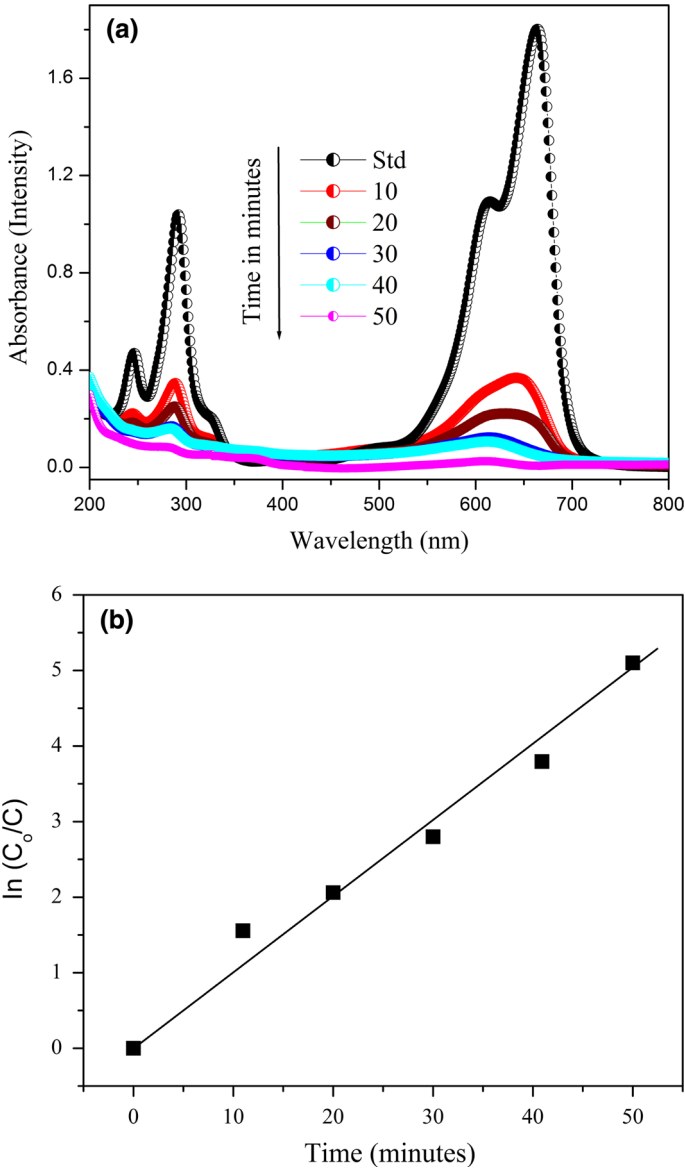
Fig. 9 **a** Changes in the absorbance spectrum of MB solution with time and **b** ln (C_o/C) versus time plot

[58] with the simultaneous occurrence of a minor photocorrosion process. The high photostability of the ZnO nanoparticles can be attributed to the efficient charge carrier separation and the increased lifetime of the charge carriers [59]. The photocatalytic degradation of some other industrial azo-dyes (10 mg/L) such as malachite green (MG), crystal violet (CV), orange II (OII), methyl orange (MO), and congo red (CR) were also investigated and the results are shown in Fig. 11.
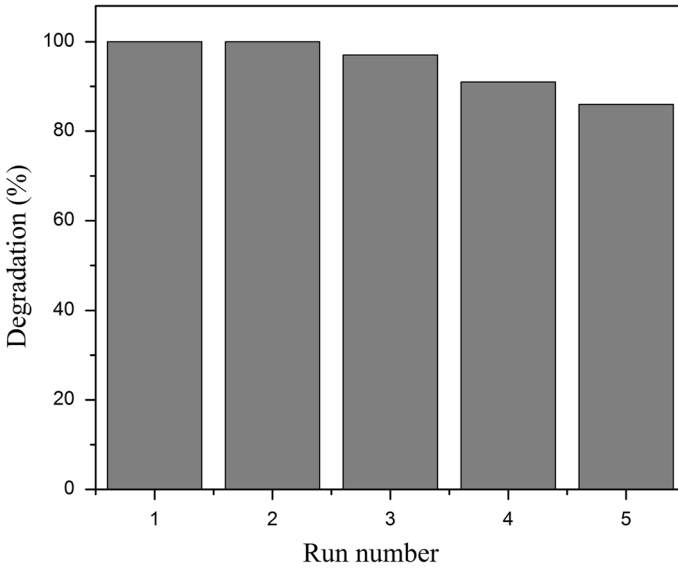
Fig. 10 Reusability of the ZnO nanoparticles (50 mL 10 mg/L MB solution, 0.05 g used ZnO and continuous air bubbling for 60 min under UV irradiation)
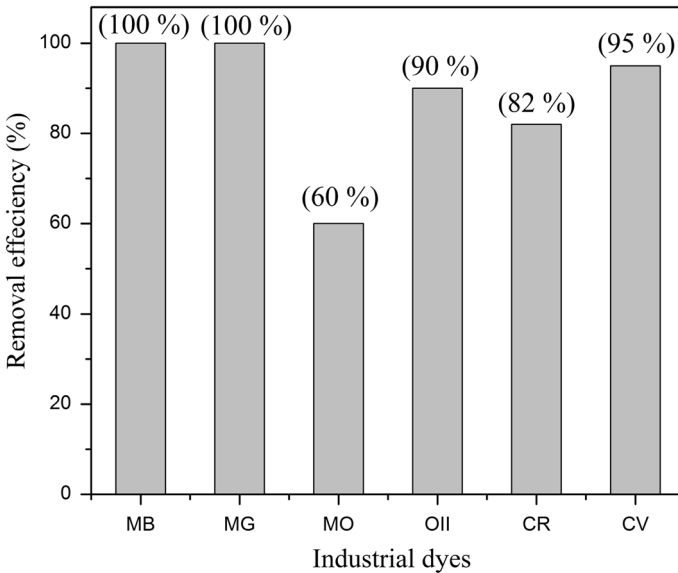

Fig. 11 Photocatalytic degradation comparison of several industrial dyes (50 mL 10 mg/L dye solution, 0.05 g ZnO and continuous air bubbling under UV irradiation for 60 min)

It can be seen that the efficiency of photo degradation of MO, OII, and CR was lower than that of MB, MG and CV. This can be attributed to their more complex molecular structures and variations in their photosensitization power [60, 61].

However, complete degradation (100 %) of MB and MG was observed within 50 min. The high catalytic activity of the as-synthesized ZnO nanoparticles for dye degradation is attributed to the presence of bulk crystal defects, especially oxygen vacancies in the sample. The large quantity of oxygen vacancies improves the trapping of photogenerated electrons, so that the rate of electron–hole pair recombination is significantly reduced [62].

Conclusions

Quasi spherical ZnO nanoparticles were successfully synthesized via an egg white assisted facile sol gel type wet method. The hexagonal wurtzite crystalline structure, mesoporous texture generated from the inter agglomeration of nanoparticles and the enhanced optical properties were confirmed by various analytical techniques. The ZnO nanoparticles were found to be highly active for the photodegradation of aquatic dye pollutants under UV irradiation over a low catalyst dose. Also they were found to be highly stable for the consecutive runs without loss in catalytic activity. The reusability can be attributed to its high photostability against photocorrosion.

References

1. S. A. Khayyat, M. Abaker, A. Umar, M. O. Alkattan, N. D. Alharbi, and S. Baskoutas (2012). *J. Nanosci. Nanotechnol.* **12**, 8453.
2. Z. L. Wang (2008). *ACS Nano* **2**, 1987.
3. A. Belaidi, Th Dittrich, D. Kieven, J. Tornow, K. Schwarzburg, M. Kunst, N. Allsop, M-Ch Lux-Steiner, and S. Gavrilov (2009). *Sol. Energy Mater. Sol. Cells* **93**, 1033.
4. Q. Zhang, C. Xie, S. Zhang, A. Wang, B. Zhu, L. Wang, et al. (2005). *Sens Actuators B* **110**, 370.
5. S. Z. Kang, T. Wu, X. Li, and J. Mu (2010). Colloids Surf. A. *Eng. Aspects* **369**, 268.
6. T. Aoki, Y. Hatanaka, and D. C. Look (2000). *Appl. Phys. Lett.* **76**, 3257.
7. D. Qian, J. Z. Jiang, and P. L. Hansen (2003). *Chem. Commun.* **9**, 1078.
8. K. Vignesh, A. Suganthi, M. Rajarajan, and S. A. Sara (2012). *Powder Technol.* **224**, 331.
9. J. L. Yang, S. J. An, W. I. Park, G. Y. Yi, and W. Choi (2004). *Adv. Mater.* **16**, 1661.
10. L. Armelao, G. Bottaro, M. Pascolini, M. Sessolo, E. Tondello, M. Bettinelli, and A. Speghini (2008). *J. Phys. Chem. C* **112**, 4049.
11. L. Y. Yang, S. Y. Dong, J. H. Sun, J. L. Feng, Q. H. Wu, and S. P. Sun (2010). *J. Hazard. Mater.* **179**, 438.
12. S. A. Studenikin, N. Golego, and M. Cocivera (2000). *J Appl Phys* **87**, 2413.
13. Z. W. Pan, Z. R. Dai, and Z. L. Wang (2001). *Science* **291**, 1947.
14. P. X. Gao and Z. L. Wang (2004). *Appl. Phys. Lett.* **84**, 2883.
15. Y. Liu, H. Lv, S. Li, X. Xing, and G. Xi (2012). *Dyes Pigm.* **95**, 443.
16. M. Zareie, A. Gholami, M. Bahrami, A. H. Rezaei, and M. H. Keshavarz (2013). *Mater Lett.* **91**, 255.
17. M. Pudukudy, A. Hetieqa, and Z. Yaakob (2014). *Appl. Surf. Sci.* doi:10.1016/j.apsusc.2014.07.050.
18. T. Ghoshal, S. Kar, and S. Chaudhuri (2007). *Cryst. Growth Des.* **7**, 136.
19. M. Bitenc, P. Podbrscek, Z. C. Orel, M. A. Cleveland, J. A. Paramo, R. M. Peters, and Y. M. Strzhemechny (2009). *Cryst. Growth Des.* **9**, 997.
20. D. Kim and Y. D. Huh (2011). *Mater. Lett.* **65**, 2100.

21. M. S. Mohajerani, M. Mazloumi, A. Lak, A. Kajbafvala, S. Zanganeh, and S. K. Sadrnezhaad (2008). *J. Cryst. Growth* **310**, 3621.
22. Y. Zhang, W. F. Zhang, and H. W. Zheng (2007). *Scripta Mater.* **57**, 313.
23. Z. Liu, Z. Jin, W. Li, and J. Qiu (2005). *Mater. Lett.* **59**, 3620.
24. D. Chen, X. Jiao, and G. Cheng (2000). *Solid State Commun.* **113**, 363.
25. V. Bansal, P. Poddar, A. Ahmad, and M. Sastry (2006). *J. Am. Chem. Soc.* **128**, 11958.
26. Y. L. Zou, Y. Li, J. G. Li, and W. J. Xie (2012). *Chem. Pap.* **66**, 278.
27. D. V. Vadehra, K. R. Nath, and R. Forsythe (1973). *CRC Crit. Rev. Food Technol.* **4**, 193.
28. S. Dhara and P. Bhargava (2001). *J. Am. Chem. Soc.* **84**, 3048.
29. F. Nouroozi and F. Farzaneh (2011). *J. Braz. Chem. Soc.* **22**, 484.
30. P. Thangaraj, J. Rajan, S. Durai, S. Kumar, A. R. Phanic, and G. Neri (2011). *Vaccum* **86**, 140.
31. M. Shoeb, B. R. Singh, J. A Khan, W. Khan, B. N. Singh, H. B. Singh, and A. H. Naqv (2013). *Adv. Nat. Sci.* **4**, 035015.
32. N. Daneshvar, S. Aber, M. S. Seyed Dorraji, A. R. Khatae, and M. H. Rasoulifard (2007). *Sep. Purific. Technol.* **58**, 91.
33. M. Pudukudy and Z. Yaakob (2013). *Superlattices Microstruct.* **63**, 47.
34. Z. Zhu, D. Yang, and H. Liu (2011). *Adv. Powder Technol.* **22**, 493.
35. M. Pudukudy, Z. Yaakob, B. Narayanan, A. Gopalakrishnan, and S. M. Tasirin (2013). *Superlattices Microstruct.* **64**, 15.
36. L. Sun, R. Shao, Z. Chen, L. Tang, Y. Dai, and J. Ding (2012). *Appl. Surf. Sci.* **258**, 5455.
37. Q. F. Zhang, T. P. Chou, B. Russo, S. A. Jenekhe, and G. Z. Cao (2008). *Angew. Chem. Int. Ed.* **47**, 2402.
38. T. Prakash, R. Jayaprakash, D. S. Raja, S. Kumar, N. Donatoc, D. Spadarod, and G. Neri (2013). *Sens. Actuators B* **176**, 560.
39. L. J. Song, Z. Shuo, L. Z. Quan, Z. K. Jun, C. J. Kang, and Q. J.-Hao (2012) *Trans. Nonferrous Met. Soc. China* **22**, 2459.
40. Q. Dong, H. Su, J. Xu, D. Zhang, and R. Wang (2007). *Mater. Lett.* **61**, 2714.
41. M. Hedstrom, F. Plieva, I. Y. Galaev, and B. Mattiasson (2008). *Anal. Bioanal. Chem.* **390**, 907.
42. A. J. Wooten, D. J. Werder, D. J. Williams, J. L. Casson, and J. A. Hollingsworth (2009) *J Am Chem Soc* **131**, 16177.
43. J. H. Sun, S. Y. Dong, J. L. Feng, X.-J. Yin, and X. C. Zhao (2011). *J. Mol. Catal. A* **335**, 145.
44. A. J. Reddy, M. K. Kokila, H. Nagabhushan, J. L. Rao, C. Shivakumar, B. M. Nagabhushan, and R. P. S. Chakradhar (2011). *Spectrochim. Acta A* **81**, 53.
45. S. Baskoutas and G. Bester (2010). *J. Phys. Chem. C* **114**, 9301.
46. S. Baskoutas and G. Bester (2011). *J. Phys. Chem. C* **115**, 15862.
47. Z. Huang, D. Yan, M. Yang, X. Liao, Y. Kang, G. Yin, and Y. Yao (2008). *J. Colloid Interface Sci.* **325**, 356.
48. U. Ozgur, Y. I. Alivov, C. Liu, A. Teke, M. A. Reshchikov, V. Avrutin, S. J. Cho, and H. Morkoc (2005). *J. Appl. Phys.* **98**, 041301.
49. K. Vanheusden, W. L. Warren, C. H. Seager, D. R. Tallant, J. A. Voigt, and B. E. Gnade (1996). *J. Appl. Phys.* **79**, 7983.
50. M. Pudukudy and Z. Yaakob (2014). *Solid State Sci.* **30**, 78.
51. J. Zhou, F. Zhao, Y. Wang, Y. Zhang, and L. Yang (2007). *J. Lumin.* **122–123**, 195.
52. N. Kiomarsipourn and R. S. Razavi (2013). *Ceram. Int.* **39**, 813.
53. G. Patrinoiu, M. Tudose, J. M. C. Moreno, R. Birjega, P. Budrugea, R. Ene, and O. Carp (2012). *J. Solid State Chem.* **186**, 17.
54. I. Fatimah, S. Wang, and D. Wulandari (2011). *Appl. Clay Sci.* **53**, 553.
55. A. Kajbafval, H. Ghorbani, A. Paravar, J. P. Samberg, E. Kajbafvala, and S. K. Sadrnezhaad (2012). *Superlattices Microstruct.* **51**, 512.
56. Y. J. Xu, Y. B. Zhuang, and X. Z. Fu (2010). *J. Phys. Chem. C* **114**, 2669.
57. K. Thongsuriwong, P. Amornpitoksuk, and S. Suwanboon (2013). *Adv. Powd. Tech.* **24**, 275.
58. T. Warang, N. Patel, A. Santini, N. Bazzanella, and A. Kale (2012). *Appl. Catal. A* **423–424**, 21.
59. M. Khatamian, A. A. Khandar, B. Divband, M. Haghighi, and S. Ebrahimiaslc (2012). *J. Mol. Catal. A* **365**, 120.
60. M. Pudukudy and Z. Yaakob (2014). *Appl. Surf. Sci.* **292**, 520.
61. M. Pudukudy, Z. Yaakob, R. Rajendran, and T. Kandaramath (2014). *React. Kinet. Mech. Catal.* **112**, 527.
62. Q. Xiao and L. Ouyang (2009). *J. Alloys Compd.* **479**, L4.